Title
Mebendazole Potentiates Radiation Therapy in Triple-Negative Breast Cancer

Journal
International Journal of Radiation Oncology • Biology • Physics, 103(1)

ISSN
0360-3016

Authors
Zhang, Le
Bochkur Dratver, Milana
Yazal, Taha
et al.

Publication Date
2019

DOI
10.1016/j.ijrobp.2018.08.046

Peer reviewed

HHS Public Access

Author manuscript

Int J Radiat Oncol Biol Phys. Author manuscript; available in PMC 2020 January 01.

Published in final edited form as:

Int J Radiat Oncol Biol Phys. 2019 January 01; 103(1): 195–207. doi:10.1016/j.ijrobp.2018.08.046.

Mebendazole Potentiates Radiation Therapy in Triple-Negative Breast Cancer

Le Zhang, MD, PhD[#*], **Milana Bochkur Dratver**[#*], **Taha Yazal, BS**[*], **Kevin Dong, BS**[*], **Andrea Nguyen, BS**[*], **Garrett Yu, BS**[*], **Amy Dao**[*], **Michael Bochkur Dratver**[*], **Sara Duhachek-Muggy, PhD**[*], **Kruttika Bhat, PhD**[*], **Claudia Alli, PhD**[*], **Frank Pajonk, MD, PhD**[*,†], and **Erina Vlashi, PhD**[*,†]

[*]Department of Radiation Oncology, David Geffen School of Medicine, University of California, Los Angeles, Los Angeles, California

[†]Jonsson Comprehensive Cancer Center, University of California, Los Angeles, Los Angeles, California

[#] These authors contributed equally to this work.

Abstract

Purpose: The lack of a molecular target in triple-negative breast cancer (TNBC) makes it one of the most challenging breast cancers to treat. Radiation therapy (RT) is an important treatment modality for managing breast cancer; however, we previously showed that RT can also reprogram a fraction of the surviving breast cancer cells into breast cancer—initiating cells (BCICs), which are thought to contribute to disease recurrence. In this study, we characterize mebendazole (MBZ) as a drug with potential to prevent the occurrence of radiation-induced reprogramming and improve the effect of RT in patients with TNBC.

Methods and Materials: A high-throughput screen was used to identify drugs that prevented radiation-induced conversion of TNBC cells into cells with a cancer-initiating phenotype and exhibited significant toxicity toward TNBC cells. MBZ was one of the drug hits that fulfilled these criteria. In additional studies, we used BCIC markers and mammosphere-forming assays to investigate the effect of MBZ on the BCIC population. Staining with propidium iodide, annexin-V, and γ-H2AX was used to determine the effect of MBZ on cell cycle, apoptosis, and double-strand breaks. Finally, the potential for MBZ to enhance the effect of RT in TNBC was evaluated in vitro and in vivo.

Results: MBZ efficiently depletes the BCIC pool and prevents the ionizing radiation–induced conversion of breast cancer cells into therapy-resistant BCICs. In addition, MBZ arrests cells in the G2/M phase of the cell cycle and causes double-strand breaks and apoptosis. MBZ sensitizes TNBC cells to ionizing radiation in vitro and in vivo, resulting in improved tumor control in a human xenograft model of TNBC.

Reprint requests to: Erina Vlashi, PhD, Department of Radiation Oncology, David Geffen School of Medicine at UCLA, 10833 Le Conte Ave, Los Angeles, CA 90095-1714. Tel: (310) 825-3064; evlashi@mednet.ucla.edu.

Conflict of interest: none.

Supplementary material for this article can be found at https://doi.org/10.1016/j.ijrobp.2018.08.046.

Conclusions: The data presented in this study support the repurposing of MBZ as a combination treatment with RT in patients with TNBC.

Introduction

Breast cancer (BC) is a heterogeneous group of diseases that is clinically managed based on the pathologic and biological features of the disease. Positivity for estrogen receptor (ER+), progesterone receptor (PR+), and epidermal growth factor receptor 2 (HER2+) in most patients with BC allows for inclusion of effective, targeted hormonal or HER-directed therapies in the treatment regimen of these subgroups of patients with BC. However, 10% to 20% of patients with BC lack expression of ER, PR, and HER2 and receive a diagnosis of triple-negative BC (TNBC). The lack of known targetable receptors, or molecular targets, in patients with TNBC makes it one of the most challenging cancers to treat.

Currently, the only available treatments for TNBC involve chemotherapy and radiation therapy (RT), after surgery. However, even with aggressive chemoradiation regimens, ~ 70% of patients with TNBC are left with residual disease that recurs with visceral metastatic disease, which results in significantly lower overall survival compared with that of patients without TNBC.[1] Therefore, novel drugs that are effective against TNBC models are urgently needed.

BCs are organized hierarchically, with a subpopulation of BC cells, also known as BC-initiating cells (BCICs), having tumor-initiating potential, whereas the rest of the cells in the tumor lack this feature.[2,3] In addition to their tumor-initiating potential, BCICs are also thought to be relatively resistant to chemotherapy and RT,[4–6] the only treatment modalities available for managing TNBCs.

Several surface and functional markers can prospectively identify cell populations enriched for BCICs.[2] We have shown that BCICs have low proteasome activity. The use of a fluorescent reporter system that reports for cells with low proteasome activity via accumulation of a fluorescent protein (ZsGreen) fused to a degron (cODC) that is recognized and destroyed by the 26S proteasome has been used to identify cancer initiating cells (CICs) in several solid tumor types, including BC.[7–12] Specifically, BC in vivo limiting dilution assays, considered the gold standard for demonstrating a CIC cell phenotype, have demonstrated the relative enrichment in BCICs in the cancer cell population, with low proteasome activity in 3 different BC cell lines: MCF7-EP (ER^+), MCF10Ca1h (ER^+), and MDA-MB-231 (basal TNBC).[8,13]

In addition, we have used the low-proteasome activity reporter for BCICs in combination with other marker systems for BCICs and extensive functional in vitro and in vivo assays. Our results have shown that exposure to ionizing radiation (IR) can dedifferentiate surviving non-tumorigenic BC cells into BCICs[14] and that TNBCs contain a larger proportion of intrinsic BCICs compared with the other subtypes of BC. Others have reported IR-induced dedifferentiation for lymphoma,[15] hepatocellular carcinoma,[16] and non-small cell lung cancer.[17] IR-induced dedifferentiation of cancer cells into CICs is not unique to IR; other

cellular stressors such as low pH,[18] hypoxia,[19] inflammation,[20] and chemotherapy[21] have also been shown to induce dedifferentiation of surviving cancer cells.

These findings suggest that unless current anticancer treatments (including IR) are 100% efficient at eliminating all the existing BC cells in the primary tumor, a fraction of surviving cells have the ability to activate a dedifferentiation program, convert into CICs, and cause recurrence. Therefore, the prevailing assumption that eliminating the intrinsic BCICs will result in cancer cures is no longer adequate because it becomes clear that strategies that will interfere with the process of therapy-induced dedifferentiation will need to be developed.

To this end, we performed a high-throughput screen for compounds that inhibit IR-induced dedifferentiation in a TNBC line. We identified several drugs that belong to the anthelminthic group of drugs to be potent inhibitors of IR-induced dedifferentiation.

We chose to further pursue study of mebendazole (MBZ) because it has several desirable characteristics of an anticancer drug: (1) MBZ is very toxic to TNBC cells in vitro; (2) MBZ is approved by the U.S. Food and Drug Administration for the treatment of nematode infections; (3) MBZ is an efficient inhibitor of IR-induced dedifferentiation; and (4) MBZ has a very favorable toxicity profile in humans even at high doses administered over lengthy periods of time.[22] MBZ (methyl 5-benzoyl-2-benzimidazole-carbamate) is a truly broad-spectrum anthelminthic drug and is part of a class of structurally related, tubulin-disrupting drugs (benzimidazoles) that have been used to treat helminthic disease in humans around the world. MBZ also has efficacy against different types of solid tumors in vitro and in vivo, such as lung cancer,[23] melanoma,[24] colon cancer,[25] glioblastoma multiforme,[26] medulloblastoma,[27] and head and neck squamous cell carcinoma.[28] However, MBZ has never been tested in TNBC models. For these reasons, we hypothesized that MBZ may radiosensitize TNBC cells to IR and have antitumor effect in TNBC.

Methods and Materials

Cell culture

Human MCF7, T47D, and MDA-MB-231 BC cell lines were purchased from American Type Culture Collection (Manassas, VA). Human SUM159PT BC cell lines were purchased from Asterand (Detroit, MI). SUM159PT-ZsGreen-cODC, MCF7-ZsGreen-cODC, T47D-ZsGreen-cODC, and MDA-MB-231-ZsGreen-cODC were obtained as described by Vlashi et al.[7] SUM159PT cells were cultured in log-growth phase in F12 Medium (Invitrogen, Carlsbad, CA) supplemented with 5% fetal bovine serum (Sigma-Aldrich, St. Louis, MO) and penicillin (100 units/mL) and streptomycin (100 μg/mL) cocktail (Invitrogen), 5 μg/mL insulin (Eli Lilly, Indianapolis, IN), 0.5% 1M hydroxyethyl piperazineethanesulfonic acid (Invitrogen), and 1 μg/mL hydrocortisone (Pfizer, New York, NY). T47D and MDA-MD-231 cells were cultured in log-growth phase in Dulbecco's Modified Eagle Medium (Invitrogen) supplemented with 10% fetal bovine serum and penicillin (100 U/mL) and streptomycin (100 μg/mL) cocktail. MCF7 cells were cultured in log-growth phase in Minimum Essential Media Alpha (Invitrogen) supplemented with 10% fetal bovine serum and penicillin (100 U/mL) and streptomycin (100 μg/mL) cocktail, nonessential amino acids

(1 ×; NEAA, Invitrogen), 1 mM sodium pyruvate (Invitrogen), and 5 μg/mL insulin (Eli Lilly). All cells were grown in a humidified incubator at 37°C with 5% CO_2.

High-throughput screening

For primary screening of drug libraries, ZsGreen-cODC-negative SUM159 cells (Asterand Bioscience) were sorted by high-speed fluorescence activated cell sorting (FACSAria I/II). Concurrently, low-evaporation 384-well plates were filled by a manifold liquid dispenser (Multidrop 384, Thermo LabSystems, Beverly, MA) with 35 μL media per well (F-12, hydrocortisone (100 mg/2 mL), 5% fetal bovine serum, 1% penicillin-streptomycin, 0.1% insulin, and 1 M 4-(2-Hydroxyethyl)piperazine-1-ethanesulfonic acid (HEPES). Using a liquid handler (Biomek FX, Beckman Coulter, Brea, CA) with a custom pin tool (V&P Scientific, San Diego, CA), 320 unique compounds (500 nL each from 1-mM stocks in neat dimethyl sulfoxide [DMSO]) were then transferred to each 384-well plate according to predefined plate maps. The other 64 wells received an equal volume of dimethyl sulfoxide (DMSO) alone, serving as negative controls. After resuspension of cells in media at a concentration of 200,000 cells/mL, 15 μL cell suspension (3000 cells) was plated into each well of the prefilled 384-well plates. After completion of cell plating, 384-well plates were kept at 37°C, 5% CO_2.

Twenty-four hours after plating, cells were irradiated with 8 Gy. Five days later, 10 μL Hoechst 33342 solution (25 μg/mL) was added to the cells. The plates were incubated at 37°C, 5% CO_2, for 1 hour. Plates were scanned using an Acumen Mark III laser-scanning cytometer (TTP Labtech, Melbourn, United Kingdom). Laser scanning with a 488-nm laser was used for detection of cells expressing the fusion protein, ZsGreen-cODC. Additionally, scanning with a ultraviolet (UV) laser at 405 nm allowed for detection of Hoechst-stained nuclei, giving a measure of total viable cells.

Z score statistics were used for hit identification: For every well of each 384-well plate, a <mi> score <mi> was calculated for both the ZsGreen-cODC-positive count and the total viable cell count. The population, characterized by the parameters μ and σ, consists of the 64 negative controls in each plate. Hits for inhibitors of dedifferentiation were defined as compounds with both (1) a ZsGreen-cODC-positive <mi> score ≤ -2.0 and (2) a total viable cell <mi> score ≥ -1.0. Hits meeting these criteria from the primary screens were tested in secondary screens.

Because of the presence of replicates in the secondary screen set-up, the <mi> score method of identifying hits from the primary screen was not used. Instead, verification of hits in the secondary screen used Student’s t test to consider the compound-specific variances. A Bonferroni correction for multiple comparisons was used to maintain a false-positive rate of <0.05 within each secondary screen.

ATPlite viability assay

ATPlite 1step Luminescence Assay System (PerkinElmer, Waltham, MA) was used to assess cell viability after treatment with MBZ. This assay measures proliferation or cytotoxicity in mammalian cells based on the production of light caused by the reaction of adenosine triphosphate (ATP) with added luciferase and D-luciferin. Cells were removed from tissue

culture plates via trypsinization, counted, and plated on 96-well plates at 10,000 cells per well in 100 μL of growth media. After the cells were allowed to attach overnight, they were treated with MBZ at indicated concentrations. At different time points after treatment with MBZ, a 100-μL per well of ATPlite substrate was added to each well. Next, 100 μL of the reaction mixture was transferred to opaque, white, 96-well plates, and the resulting luminescence was analyzed with the use of a fluorescence/luminescence plate reader (SpectraMax M5, Molecular Devices, Sunnyvale, CA) at room temperature.

ALDH1 assay

Ginestier et al previously reported that breast cancer stem cells (BCSCs) could be isolated based on their high aldehyde dehydrogenase 1 (ALDH1) activity.[3] The ALDEFLUOR kit (STEMCELL Technologies, Vancouver, BC, Canada; http://www.stemcell.com/) was used to identify cells with ALDH1 activity. Cells obtained from BC monolayer (SUM159PT and MDA-MB-231) were suspended in ALDEFLUOR assay buffer containing ALDH1 substrate and incubated for 40 minutes at 37°C. As a negative control for each sample of cells, an aliquot was treated with 50 mmol/L diethylaminobenzaldehyde, a specific ALDH1 inhibitor. The flow cytometry analysis gates were established using ALDEFLUOR-stained cells treated with diethylaminobenzaldehyde as negative controls.

Mammosphere-forming assays

To assess mammosphere-forming capacity, cells were trypsinized and plated in “sphere media” (Dulbecco’s Modified Eagle’s Medium F-12, 0.4% bovine serum albumin (BSA) [Sigma], 10 mL/500 mL B27 [Invitrogen] 5 μg/mL bovine insulin [Sigma], 4 μg/mL heparin [Sigma], 20 ng/mL fibroblast growth factor 2 [bFGF, Sigma], and 20 ng/mL epidermal growth factor, Sigma) into 96-well ultralow adhesion plates, at a range of cell densities. Growth factors, epidermal growth factor and bFGF, and heparin were added every 3 days, and the cells were allowed to form spheres for approximately 2 to 3 weeks. The number of spheres formed per well was then counted and expressed as a percentage of the initial number of cells plated.

Measuring mitochondrial membrane potential assay and reactive oxygen species

To measure mitochondrial membrane potential, 200,000 cells per well were plated in 6-well plates, allowed to attach overnight, and treated with MBZ 24 hours later. After drug treatment, cells were washed twice with phosphate-buffered saline (PBS), and the mitochondrial membrane potential was measured via the fluorescent dye, tetramethylrhodamine methyl ester (TMRM). Cells were incubated with 50 nM TMRM for 30 minutes in PBS at 37°C, trypsinized, and washed with fresh media. After resuspending in PBS, cells were analyzed by flow cytometry using a MACSQuant Analyzer (Miltenyi Biotec) for TMRM fluorescence. The mean fluorescence intensity was recorded for all the experimental groups. Three biologically independent experiments were performed.

For measuring reactive oxygen species (ROS) after MBZ treatment, 5 μM per well of the CellROX Deep Red Reagent (ThermoFisher Scientific) was added to the growth media at the indicated time points, and the cells were incubated for 30 minutes at 37°C. After the cells were washed with PBS, the cells were detached, resuspended in PBS, and analyzed by

flow cytometry using a MACSQuant Analyzer (Miltenyi Biotec) for CellROX Deep Red fluorescence (Excitation 635 nm).

Annexin-V flow cytometry

For measuring the fraction of cells undergoing apoptosis at different time points after MBZ exposure, 400,000 cells per well were plated in 6-well plates and allowed to adhere overnight. The next day, DMSO or MBZ was added at the indicated concentrations. At the indicated time points, the cells were removed with Accutase (Sigma), and the cell pellet was washed 1 time with ice-cold PBS. The cells were then resuspended in annexin-binding buffer (10 mM HEPES, 140 mM NaCl, 2.5 mM $CaCl_2$, pH 7.4) at ~ 1×10^6 cells/mL. Then 5 μL of Annexin V, Alexa Fluor 647 conjugate (ThermoFisher Scientific, A23204), or Annexin V-FITC conjugate (BioLegend) was added per 100 μL of cell suspension. Cells were incubated at room temperature for 15 minutes, and 400 μL of annexin-binding buffer was added. The cells were kept on ice until ready for analysis by flow cytometry.

γ-H2AX flow cytometry

Cells treated with MBZ were fixed with 4% formaldehyde for 10 minutes at 37°C, and the culture plates were chilled on ice for 1 minute. The fixative was then removed, and the cells were permeabilized with 90% methanol for 30 minutes on ice. The cells were removed and resuspended to 107 nucleated cells per 100 μL of staining buffer (PBS, pH 7.2, 0.5% bovine serum albumin, and 2 mM ethylenediaminetetraacetic acid), and 10 μL of the anti-H2AX pS139-APC antibody (130-107-586, Miltenyi Biotec) was added to the cell suspension. After being mixed well, the cells were incubated with the antibody for 30 minutes in the dark at room temperature. After washing with PBS, cells were resuspended in PBS and analyzed by flow cytometry using a MACSQuant Analyzer (Miltenyi Biotec) for allophycocyani fluorescence.

Cell cycle analysis

SUM159PT cells were treated with MBZ at the indicated concentrations. After 24 hours, cells were removed and counted, and 1×10^6 cells were spun down for 5 minutes at 300 g at 4°C. The pellet was resuspended in 1 mL of hypotonic DNA staining buffer (3.8 mM sodium citrate/0.3% Triton-x 100/150 μM propidium iodide/1.5 μM ribonuclease A in distilled H_2O). Resuspended cells were kept at room temperature for 15 minutes before being analyzed on a BD-LSRFortessa X-20 analyzer. ModFit LT 5.0 was used to model DNA cell cycle phases. Pre-gating was used for doublet discrimination by plotting phycoerythrin-area (PE-A) versus phycoerythrin-width (PE-W). With the selection of the nonaggregate populations, the ModFit manual analysis model was used in the diploid setting to calculate percentages for each phase of the cell cycle.

Clonogenic survival assays

For clonogenic survival assays, cells were plated in 10-cm dishes and allowed to adhere overnight. On the next day, cells were treated with DMSO or MBZ at the indicated concentrations. After 24 hours, cells were trypsinized, counted, and irradiated and replated at specific cell numbers (depending on the radiation dose) into 10-cm petri dishes using

standard culture media. Two weeks later, cells were fixed with 70% ethanol and stained with crystal violet. Colonies containing more than 50 cells were counted and normalized to their corresponding unirradiated control. Data points were fitted using a linear-quadratic model (GraphPad Prism, version 5.0).

Irradiation

Cell culture plates were irradiated at room temperature using an experimental x-ray irradiator (Gulmay Medical Inc, Suwanee, GA) at a dose rate of 2.789 Gy/min for the time required to apply a prescribed dose. The x-ray beam was operated at 300 kV and hardened using 4-mm Be, 3-mm Al, and 1.5-mm Cu filters. Corresponding controls were sham irradiated.

Animals

Immune-compromised, 6-week-old NOD.Cg-*Prkdc*^{scid} *Il2rg*^{tm1Wjl}/SzJ (NSG) mice, originally obtained from The Jackson Laboratories (Bar Harbor, ME), were re-derived, bred, and maintained in a pathogen-free environment in the American Association of Laboratory Animal Care—accredited Animal Facilities in accordance with all local and national guidelines for the care of animals.

Tumor xenotransplantation and treatment

The 10^6 SUM159PT cells per inoculum mixed with 50% Matrigel (BD Matrigel Basement Membrane Matrix, Fisher Scientific) were implanted subcutaneously into both thighs of 6-week-old female NSG mice. When tumors reached an average diameter of 5 mm, the mice were treated intraperitoneally with MBZ at the indicated doses, 3 hours before irradiation. For intraperitoneal treatments with MBZ, the drug was prepared fresh daily by first dissolving it in DMSO and then suspending it in a 1% Cremophor/water mixture before administration. Control mice were treated with the equivalent DMSO/1% Cremophor/water solution.

To deliver radiation treatment, 1 of the tumor-bearing thighs of mice was treated with 10 Gy using an experimental x-ray irradiator (Gulmay Medical Inc) at a dose rate of 5.519 Gy/min for the time required to apply the prescribed dose. The rest of the mouse, including the opposite tumor-bearing thigh, was shielded with 10-mm lead blocks. The x-ray beam was operated at 300 kV and hardened using 4-mm Be, 3-mm Al, and 1.5-mm Cu filters. MBZ treatment was continued every day for 3 consecutive weeks on a 5-days-on, 2-days-off schedule. Tumor volume (T) = $0.5 \times L \times W^2$, where L is the longest axis (in millimeters) and W is the axis perpendicular to L (in millimeters). The “% tumor growth” = $100 + ([\Delta T/T_{initial}] \times 100)$, where ΔT = mean tumor volume on the study day of interest – mean initial tumor volume ($T_{initial}$) and all the values are normalized to setting $T_{initial} = 100\%$.

Statistics

All data are represented as mean ± standard error mean of at least 3 biologically independent experiments. A P value of < .05 in a 2-sided t test indicated a statistically significant difference.

Results

High-throughput screening for inhibition of radiation-induced dedifferentiation in TNBC identifies anthelminthic drugs

Using the reporter system for BCICs with low proteasome activity (ZsGreen-cODC), in combination with functional assays, we have shown that IR can dedifferentiate a fraction of the surviving noninitiating BC (NIBC) cells into BCICs.[14] In this study, we confirmed these findings in 4 BC lines representing different subsets of BC: luminal (MCF7 and T47D), basal (MDA-MB-231), and claudin-low (SUM159PT). In agreement with our previous findings, exposure to IR efficiently dedifferentiated ZsGreen-cODC-negative (ZSG-neg) NIBC cells into ZsGreen-cODC-positive (ZSG-pos) BCICs in a dose-dependent manner (Fig. 1 and Fig. E1 A-C; available online at https://doi.org/10.1016/j.ijrobp.2018.08.046). Importantly, we observed that ZSG-neg cells sorted from 2 TNBC lines, MDA-MB-231 and SUM159PT, dedifferentiated more efficiently into ZSG-pos BCICs, either spontaneously (Fig. 1A, black bars) or after exposure to IR (Fig. 1A), compared with the luminal lines (MCF7 and T47D; Fig. 1A). Of note, IR-induced dedifferentiation peaks approximately 5 days after exposure to IR (Fig. E1A-C; available online at https://doi.org/10.1016/j.ijrobp.2018.08.046), and fractionated regimens (often used in the clinic for treating BC) of 5 daily fractions of either 2 Gy or 3 Gy were less efficient at inducing dedifferentiation compared with a single dose of 8 Gy (Fig. 1A, striped bars, and Fig. E1D; available online at https://doi.org/10.1016/j.ijrobp.2018.08.046).

Given the significantly poorer prognosis of TNBCs (mainly because of the lack of druggable targets), we decided to perform a high-throughput screen for identifying drugs that prevent IR-induced dedifferentiation in TNBC. For this purpose, we used the TNBC line SUM159PT stably expressing ZsGreen-cODC fluorescent reporter for BCICs with low proteasome activity. SUM159PT-ZSG-pos BCICs were depleted via high-speed FACS. The SUM159PT-ZSG-neg cells were plated on 384-well plates already containing a library of drugs and were irradiated the next day. Five days later, cells were stained with a viability dye, and the number of viable cells and the number of IR-induced ZSG-pos cells was determined via a laser-scanning cytometer (data not shown).

The high-throughput screen resulted in identification of several anthelminthic drugs as efficient inhibitors of IR-induced dedifferentiation. Subsequently, a larger group of anthelminthic drugs (20 drugs) was tested in a secondary screen for their effect in inhibiting IR-induced dedifferentiation in vitro (Fig. 1B).

Of note, although 7 of the 20 anthelminthic drugs tested in the secondary screen inhibited IR-induced generation of ZSG-pos cells (Fig. 1B, dark bars), the rest of the anthelminthics had no effect or promoted, rather than inhibited, IR-induced dedifferentiation (Fig. 1B, light bars). Of the anthelminthic drugs that inhibited IR-induced dedifferentiation with a ZsGreen <mi> score <−1 (Fig. 1B, top panel, dotted horizontal line), we decided to further test MBZ (trade name, Vermox; Fig. 1C) for its effect on TNBC cells for 3 reasons. First, in addition to inhibiting dedifferentiation (Fig. 1B, top panel, and Fig. E1D; available online at https://doi.org/10.1016/j.ijrobp.2018.08.046), MBZ showed the highest toxicity to the bulk of TNBC cells (Fig. 1B, bottom panel). Second, it has anti-cancer activity in vitro and in vivo

in several types of solid tumor models[29]; however, it has never been tested in BC. Third, MBZ has a very favorable in vivo toxicity profile in patients treated for helminthic infections and can be safely administered to adults and children at high doses over extended periods.[22]

MBZ toxic to TNBC cells, inhibits self-renewal and IR-induced dedifferentiation

The observation of the high toxicity of MBZ (at 10 μM concentration) on the SUM159PT BC line in the high-throughput screening experiments (Fig. 1B, bottom panel) prompted us to determine the EC50 (effective concentration that results in 50% cell death) through a dose-response curve. We observed a potent dose-dependent toxic effect of MBZ on 2 different TNBC lines, SUM159PT and MDA-MB-231, and 1 luminal BC line, MCF7 (Fig. 2A and Fig. E2A; available online at https://doi.org/10.1016/j.ijrobp.2018.08.046), as well as BCIC-enriched, serum-free mammosphere cultures (Fig. 2B), as early as 24 hours after exposure to a single dose of MBZ. Both monolayer and mammosphere cultures reached an EC50 by 48 hours after MBZ treatment: ~0.35 μM for monolayers and ~0.4 μM for mammospheres (Fig. 2A, 2B, dashed horizontal line). Of note, although the monolayer cultures reached an EC80 by 48 hours (Fig. 2A, 2B, horizontal dotted line), the mammosphere cultures enriched for BCICs only reached EC80 after 72 hours of exposure.

We next analyzed the effect of MBZ on the BCIC population by using the activity of the ALDH1 enzyme, which is often used as a reliable marker for BCICs.[3] A single treatment with MBZ dose-dependently decreased the fraction of ALDH1-pos BCICs 5 days after treatment (Fig. 2C and Fig. E2B; available online at https://doi.org/10.1016/j.ijrobp.2018.08.046). In addition, MBZ treatment resulted in a significant depletion of functional BCICs capable of self-renewal, as measured by a mammosphere-forming assay in 2 TNBC lines, SUM159PT and MDA-MB-231 (Fig. 2D). These results demonstrate that exposure to MBZ results in depletion of the intrinsic BCIC pool in TNBC cells.

MBZ was initially identified as an inhibitor of IR-induced dedifferentiation in a high-throughput screen using the ZsGreen-cODC reporter for BCICs (Fig. 1B). Therefore, we also tested the effect of MBZ on inhibiting the conversion of BC cells into functional IR-induced BCICs by measuring the mammosphere-forming capacity of IR-induced ZsGreen-pos BCICs in the SUM159PT line. As shown in Figure 2E, the conversion of ZSG-neg NIBC cells into functional (capable of forming mammospheres) IR-induced BCICs is significantly inhibited by pretreatment with a single dose of MBZ 1 hour before exposure to IR (Fig. 2E and Fig. E2C; available online at https://doi.org/10.1016/j.ijrobp.2018.08.046). For comparison, we also tested 2 commonly used chemotherapeutic drugs for BC, Cytoxan (cyclophosphamide) and Adriamycin (doxorubicin), for their effect on the IR-induced conversion of NIBC into BCICs.

Interestingly, the ZsGreen marker assay for BCIC suggested that Cytoxan increases the percentage of IR-induced ZSG-pos BCICs, whereas Adriamycin caused a significant inhibition (Fig. E2D; available online at https://doi.org/10.1016/j.ijrobp.2018.08.046). However, functional mammosphere-forming assays revealed that Cytoxan causes a slight decrease in the frequency of functional IR-induced BCICs, although at much lower efficiency compared with MBZ (Fig. E2E; available online at https://doi.org/10.1016/j.ijrobp.2018.08.046). In contrast, Adriamycin was very effective at preventing the

conversion of NIBC cells into IR-induced functional BCICs (Fig. E2E; available online at https://doi.org/10.1016/j.ijrobp.2018.08.046).

Finally, MBZ has been shown to inhibit the canonical hedgehog (Hh) signaling pathway,[30] which is important for maintaining a cancer-initiating phenotype in normal and cancer cells.[31,32] We observed that a single treatment with MBZ significantly downregulates the expression of the downstream effector of Hh signaling, *GLI1* (Fig. E2F; available online at https://doi.org/10.1016/j.ijrobp.2018.08.046).

MBZ induces double-strand breaks, cell cycle arrest, and apoptosis and radiosensitizes TNBC in vitro and in vivo

The observation that MBZ efficiently inhibits IR-induced dedifferentiation led us to test whether MBZ also has a radiosensitizing effect on TNBC cells. For this purpose, BC cells were treated with a single dose of MBZ for 24 hours. After removing the drug, cells were exposed to increasing doses of IR, and the surviving fractions at each dose were compared with the untreated cells. MBZ had a significant radiosensitizing effect on 2 TNBC lines, SUM159PT and MDA-MB-231, at all radiation doses tested (Fig. 3B and Fig. E3A; available online at https://doi.org/10.1016/j.ijrobp.2018.08.046).

We then tested the effect of MBZ on tumor growth in vivo in combination with RT. In the clinic, BCs (including TNBC) are generally treated with fractionated doses on the order of 2 Gy. However, for our preclinical in vivo study, we chose a standard experimental approach and delivered a single dose of 10 Gy to established subcutaneous SUM159PT tumors.

Treatment of the tumor-bearing mice with MBZ (10 mg/kg or 20 mg/kg) for 3 weeks (5 days on, 2 days off) resulted in modest delay of tumor growth on its own (Fig. 3C, squares), but a single dose of 10 Gy significantly delayed tumor growth (Fig. 3C, empty circles). The combination of 10 Gy with 10 mg/kg of MBZ did not have any added effect on tumor growth compared with 10 Gy alone (Fig. 3C, solid triangles vs empty circles). However, the combination of a single 10-Gy treatment with 20 mg/kg of MBZ resulted in delayed tumor growth compared with 10 Gy alone (Fig. 3C, empty triangles vs empty circles). These results suggested that MBZ can also enhance the effect of RT on TNBC tumors in vivo. Importantly, no toxicity was observed from in vivo administration of 20 mg/kg MBZ for the duration of the experiment (Fig. E3B; available online at https://doi.org/10.1016/j.ijrobp.2018.08.046).

On the basis of the observed radiosensitizing effect of MBZ on TNBC cells in vitro (Fig. 3), we hypothesized that MBZ is causing cell cycle arrest in a radiosensitive phase of the cell cycle in TNBC lines. Indeed, treatment of SUM159PT cells with a single dose of MBZ for 24 hours arrests cells in the radiosensitive G2/M phase of the cell cycle (Fig. 4A and Fig. E4A; available online at https://doi.org/10.1016/j.ijrobp.2018.08.046). We also observed a statistically significant increase in γ-H2AX staining (Fig. 4B, left panel) 24 hours after MBZ treatment (Fig. 4B, right panel, light gray bars). Although not statistically significant, cells treated with MBZ for 24 hours followed by exposure to IR showed increased γ-H2AX accumulation 30 minutes after IR exposure (Fig. 4B, right panel, dark gray bars).

In general, double-strand breaks (DSBs) are caused by either direct damage to the DNA or as a secondary by-product of highly reactive oxygen species. We analyzed ROS levels after MBZ treatment at different time points, using the ROS-sensitive fluorescent dye, CellROX Deep Red, which detects general oxidative stress in a cell caused by an imbalance between production of ROS and the ability of cells to scavenge them. We observed that the increase in DSBs 24 hours after MBZ treatment (Fig. 4B) does not coincide with an increase in ROS production at this time point (Fig. E4B; available online at https://doi.org/10.1016/j.ijrobp.2018.08.046).

Finally, we analyzed the expression of apoptotic marker, Annexin-V, after exposure to MBZ. As shown in Figure 4C, a single treatment with MBZ increases the fraction of apoptotic cells in a dose- and time-dependent manner (Fig. 4C and Fig. E4C; available online at https://doi.org/10.1016/j.ijrobp.2018.08.046). Radiation alone at the clinically relevant dose of 2 Gy also induces apoptosis in a dose-dependent manner 24 hours after exposure (Fig. 4D and Fig. E4C; available online at https://doi.org/10.1016/j.ijrobp.2018.08.046). The addition of MBZ (24 hours before radiation exposure) further expands the fraction of cells undergoing apoptosis (Fig. 4E and Fig. E4C; available online at https://doi.org/10.1016/j.ijrobp.2018.08.046). Of note, treatment with 0.7 μM MBZ resulted in a similar fraction of cells undergoing apoptosis compared with treatment with 10 μM Taxol, emphasizing the significantly higher toxicity of this drug against the TNBC line compared with a commonly used chemotherapeutic in BC (Fig. E4D; available online at https://doi.org/10.1016/j.ijrobp.2018.08.046).

Apoptotic death also can lead to depolarization of mitochondrial membrane potential[33]; therefore, we also stained cells with the membrane-potential-sensitive dye TMRM at different time points after treatment with MBZ. Surprisingly, treatment with 0.7 μM MBZ led to hyperpolarization of the mitochondrial membrane potential instead of depolarization in SUM159PT cells, especially 72 hours after treatment (Fig. E4E; available online at https://doi.org/10.1016/j.ijrobp.2018.08.046).

Discussion

The anthelminthic drug MBZ has been shown to have an anticancer effect in several preclinical models of cancer[29]; however, no studies to date show its efficacy in TNBC models. In a high-throughput screen designed to identify drugs that would inhibit radiation-induced dedifferentiation of TNBC cells into cancer cells with a “stemlike” phenotype, MBZ was identified as a “hit” not only for efficiently inhibiting the radiation-induced dedifferentiation but also as a potent inducer of cell death in TNBC cells (Fig. 1).

Follow-up experiments confirmed the potent toxicity of MBZ against TNBC cells grown in differentiating cell culture conditions (as monolayers in the presence of serum; Fig. 2A) and in conditions that enrich for cells with a “cancer stem cell” phenotype and self-renewal capacity that in general are more resistant to cytotoxic treatments[34] (mammospheres; Fig. 2B). Using the ALDH1 enzymatic activity as a marker for BCICs3 (Fig. 2C) and the functional mammosphere-forming assay as a measure of self-renewal (Fig. 2D), we showed the significant effect that MBZ has on depleting BCICs in TNBC lines. This is the first

evidence that MBZ has an effect on the BCIC population in TNBC, although a recent report showed similar effects for another benzimidazole anthelminthic, flubendazole.[35]

The toxic effect of MBZ on TNBC cells was discovered in an attempt to identify drugs that inhibit radiation-induced dedifferentiation of TNBC cells into BCICs.[14] Comparison of MBZ with 2 other commonly used chemotherapeutics for the treatment of BC, Adriamycin (doxorubicin) and Cytoxan (cyclophosphamide), revealed that Adriamycin is also very effective at inhibiting radiation-induced dedifferentiation of TNBC cells into BCICs, whereas Cytoxan had minimal effect (Fig. E2 C-E; available online at https://doi.org/10.1016/j.ijrobp.2018.08.046). These data suggested that, when combined with RT, Adriamycin could also efficiently inhibit radiation-induced dedifferentiation of BC cells. However, Adriamycin is known for inducing cardiotoxicity.[36,37] This effect potentially limits its therapeutic effect in combination with breast RT, the delivery of which also poses increased cardiovascular risks for patients with BC because of the necessary involvement of cardiac substructures in the irradiation field, depending on the location of the breast tumor.[38] Therefore, we hypothesized that the combination of MBZ with RT would improve tumor control without significant toxicity.

In contrast to the potent toxicity of MBZ as a single agent on TNBC cells in vitro (Fig. 2A, 2B), MBZ had only a modest effect on tumor growth in vivo in a human TNBC tumor model (Fig. 3C, squares). However, MBZ acted as a radiosensitizer to RT in vitro (Fig. 3A, 3B) and in vivo (Fig. 3C), without any additional in vivo toxicity (Fig. E3; available online at https://doi.org/10.1016/j.ijrobp.2018.08.046). The maximum weight loss was 10% of the initial body weight at the end of the assessment period (30 days after initiation of treatment), and no difference in weight loss was observed between the treated and control groups. Although the lack of toxicity in this short-term experimental treatment with MBZ does not necessarily reflect long-term toxicity, other studies have demonstrated the favorable toxicity profile of MBZ over long periods.[39]

Other studies have shown that MBZ potentiates the effect of different chemotherapeutics in different tumor models[28,40]; however, to the best of our knowledge, this is the first time that MBZ has been used in combination with RT in any tumor type. These results support a high potential for MBZ to improve tumor control by RT in TNBC.

In search of a mechanism by which MBZ enhances the effect of RT on TNBC cells, we investigated the effect of MBZ on cell cycle distribution, apoptosis, generation of ROS, and the induction of DSBs. Benzimidazole anthelminthics have been shown to cause cell cycle arrest in different types of cancers,[41,42] including BC cells,[35] and MBZ specifically causes cell cycle arrest in lung cancer and melanoma cell lines.[23,40] In agreement with these studies, we showed that MBZ causes cell cycle arrest in the radiosensitive G2/M phase of the cell cycle in TNBC cells (Fig. 4A). The MBZ-induced cell cycle arrest was followed by significant induction of apoptotic cell death in a dose- and time-dependent manner (Fig. 4C). These results were also in agreement with other studies showing apoptosis as the primary mode of cell death by MBZ in other tumor types, such as melanoma,[24,40] lung cancer,[23,43] and medulloblastoma.[30]

Tubulin depolymerization has been shown to be a major target for benzimidazoles, including MBZ.[44–46] Although we did not investigate the effect of MBZ on tubulin in TNBC lines, others have shown, in different types of cancer cell lines, that MBZ induces depolymerization of tubulin and inhibits normal spindle formation, resulting in mitotic arrest and apoptosis.[24,26,30,43,47,48]

IR exerts its cytotoxic effect primarily by causing DSBs, either by interacting directly with the DNA or via the generation of highly reactive oxygen species that in turn cause DNA damage that the cell cannot repair. Therefore, we also measured the ROS levels in cells treated with MBZ, but we did not detect significant differences (Fig. E4B; available online at https://doi.org/10.1016/j.ijrobp.2018.08.046), suggesting that the radiosensitizing effect of MBZ was not the result of increased ROS induction. However, some reports indicate that benzimidazole compounds can intercalate into DNA and bind DNA grooves[49–51] because of their extended molecular structures containing aromatic rings (Fig. 1C). Moreover, a recent report shows that MBZ directly causes DSBs in zebrafish retina, as measured by terminal deoxynucleotidyl transferase dUTP nick end labeling staining.[52] To the best of our knowledge, the effect of MBZ on the DNA of cancer cells has never been reported.

Here, we show that a single treatment of TNBC cells with MBZ causes a significant increase in DSB, as measured by γ-H2AX staining 24 hours after exposure to MBZ (Fig. 4B). The increase in the percentage of cells that arrest in the G2/M phase of the cell cycle (in which cells have double the amount of DNA and therefore higher basal DSB) and are undergoing apoptosis (accompanied by DSB formation) at 24 hours post-MBZ exposure may be contributing to the increased levels of DSB observed at this time point. However, the complete shift of the γ-H2AX staining histogram (Fig. 4B, top panel) suggests that all the cells have increased levels of γ-H2AX compared with the vehicle-treated cells.

In contrast, treatment with 0.35-μM MBZ for 24 hours causes only ~ 20% of the cells to arrest in the G2/M phase of the cell cycle (Fig. 4A), and less than 5% of the cells are undergoing apoptosis. Therefore, the increase in DSB measured by γ-H2AX after 24 hours of MBZ exposure cannot be solely explained by cell cycle arrest in G2/M or apoptotic cell death observed at this time point, suggesting the induction of direct DSB by MBZ. In addition, the recent study on zebrafish retina shows that MBZ activates ataxia telangiectasia, mutated (ATM) dependent DNA damage response and that inhibition of ATM attenuated MBZ-induced apoptosis.[52] Taken together, these results suggest that, in addition to acting as an inhibitor of radiation-induced dedifferentiation of BC cells into BCICs, the radiosensitizing effect of MBZ is also partly attributable to the increased amount of lethal DSB.

Conclusions

These findings strongly support the use of MBZ in combination with RT to improve tumor control in TNBC. MBZ is already being repositioned for treatment of diverse tumor types,[29] and we believe this combination strategy would also prove beneficial for other tumor types that are frequently treated with RT, such as medulloblastoma,[27,30,53] high-grade gliomas,[26,48,54] and, recently, head and neck squamous cell carcinoma.[28] The results presented in

this study add to the existing body of literature supporting the repurposing of MBZ for treatment of cancers. However, further preclinical studies are needed to demonstrate the utility of combination treatments of MBZ with RT to further improve outcomes in patients with cancer.

Supplementary Material

Refer to Web version on PubMed Central for supplementary material.

Acknowledgments—

The authors thank the Janis V. Giorgi Flow Cytometry Core Laboratory staff at University of California, Los Angeles, for their assistance in performing cell cycle distribution analysis.

E.V. was supported by a Junior Faculty Award from the American Society for Radiation Oncology. F.P. was supported by grants from the National Cancer Institute (1R01CA161294).

References

1. Liedtke C, Mazouni C, Hess KR, et al. Response to neoadjuvant therapy and long-term survival in patients with triple-negative breast cancer. J Clin Oncol 2008;26:1275–1281. [PubMed: 18250347]
2. Al-Hajj M, Wicha MS, Benito-Hernandez A, et al. Prospective identification of tumorigenic breast cancer cells. Proc Natl Acad Sci USA 2003;100:3983–3988. [PubMed: 12629218]
3. Ginestier C, Hur MH, Charafe-Jauffret E, et al. ALDH1 is a marker of normal and malignant human mammary stem cells and a predictor of poor clinical outcome. Cell Stem Cell 2007;1:555–567. [PubMed: 18371393]
4. Phillips TM, McBride WH, Pajonk F. The response of CD24(/low)/CD44þ breast cancer-initiating cells to radiation. J Natl Cancer Inst 2006;98:1777–1785. [PubMed: 17179479]
5. Woodward WA, Chen MS, Behbod F, et al. WNT/beta-catenin mediates radiation resistance of mouse mammary progenitor cells. Proc Natl Acad Sci U S A 2007;104:618–623. [PubMed: 17202265]
6. Li X, Lewis MT, Huang J, et al. Intrinsic resistance of tumorigenic breast cancer cells to chemotherapy. J Natl Cancer Inst 2008;100: 672–679. [PubMed: 18445819]
7. Vlashi E, Kim K, Lagadec C, et al. In vivo imaging, tracking, and targeting of cancer stem cells. J Natl Cancer Inst 2009;101:350–359. [PubMed: 19244169]
8. Stacer AC, Wang H, Fenner J, et al. Imaging reporters for proteasome activity identify tumor- and metastasis-initiating cells. Mol Imaging 2015;14:414–428. [PubMed: 26431589]
9. Lagadec C, Vlashi E, Bhuta S, et al. Tumor cells with low proteasome subunit expression predict overall survival in head and neck cancer patients. BMC Cancer 2014;14:152. [PubMed: 24593279]
10. Vlashi E, Lagadec C, Chan M, et al. Targeted elimination of breast cancer cells with low proteasome activity is sufficient for tumor regression. Breast Cancer Res Treat 2013;141:197–203. [PubMed: 24013708]
11. Hayashi K, Tamari K, Ishii H, et al. Visualization and characterization of cancer stem-like cells in cervical cancer. Int J Oncol 2014;45: 2468–2474. [PubMed: 25269542]
12. Tamari K, Hayashi K, Ishii H, et al. Identification of chemoradiation-resistant osteosarcoma stem cells using an imaging system for proteasome activity. Int J Oncol 2014;45:2349–2354. [PubMed: 25269626]
13. Tang B, Raviv A, Esposito D, et al. A flexible reporter system for direct observation and isolation of cancer stem cells. Stem Cell Reports 2015;4:155–169. [PubMed: 25497455]
14. Lagadec C, Vlashi E, Della Donna L, et al. Radiation-induced reprogramming of breast cancer cells. Stem Cells (Dayton, Ohio) 2012;30:833–844.

15. Salmina K, Jankevics E, Huna A, et al. Up-regulation of the embryonic self-renewal network through reversible polyploidy in irradiated p53-mutant tumour cells. Exp Cell Res 2010;316:2099–2112. [PubMed: 20457152]
16. Ghisolfi L, Keates AC, Hu X, et al. Ionizing radiation induces stemness in cancer cells. PloS One 2012;7:e43628. [PubMed: 22928007]
17. Gomez-Casal R, Bhattacharya C, Ganesh N, et al. Non-small cell lung cancer cells survived ionizing radiation treatment display cancer stem cell and epithelial-mesenchymal transition phenotypes. Mol Cancer 2013;12:94. [PubMed: 23947765]
18. Hjelmeland AB, Wu Q, Heddleston JM, et al. Acidic stress promotes a glioma stem cell phenotype. Cell Death Differ 2011;18:829–840. [PubMed: 21127501]
19. Conley SJ, Gheordunescu E, Kakarala P, et al. Antiangiogenic agents increase breast cancer stem cells via the generation of tumor hypoxia. Proc Natl Acad Sci U S A 2012;109:2784–2789. [PubMed: 22308314]
20. Iliopoulos D, Hirsch HA, Wang G, et al. Inducible formation of breast cancer stem cells and their dynamic equilibrium with non-stem cancer cells via IL6 secretion. Proc Natl Acad Sci USA 2011;108: 1397–1402. [PubMed: 21220315]
21. Auffinger B, Tobias AL, Han Y, et al. Conversion of differentiated cancer cells into cancer stem-like cells in a glioblastoma model after primary chemotherapy. Cell Death Differ 2014;21:1119–1131. [PubMed: 24608791]
22. El-On J Benzimidazole treatment of cystic echinococcosis. Acta Tropica 2003;85:243–252. [PubMed: 12606103]
23. Mukhopadhyay T, Sasaki J, Ramesh R, et al. Mebendazole elicits a potent antitumor effect on human cancer cell lines both in vitro and in vivo. Clin Cancer Res 2002;8:2963–2969. [PubMed: 12231542]
24. Doudican N, Rodriguez A, Osman I, et al. Mebendazole induces apoptosis via Bcl-2 inactivation in chemoresistant melanoma cells. Mol Cancer Res 2008;6:1308–1315. [PubMed: 18667591]
25. Nygren P, Fryknas M, Agerup B, et al. Repositioning of the anthelmintic drug mebendazole for the treatment for colon cancer. J Cancer Res Clin Oncol 2013;139:2133–2140. [PubMed: 24135855]
26. Bai RY, Staedtke V, Aprhys CM, et al. Antiparasitic mebendazole shows survival benefit in 2 preclinical models of glioblastoma multiforme. Neuro Oncol 2011;13:974–982. [PubMed: 21764822]
27. Bodhinayake I, Symons M, Boockvar JA. Repurposing mebendazole for the treatment of medulloblastoma. Neurosurgery 2015;76: N15–N16.
28. Zhang F, Li Y, Zhang H, et al. Anthelmintic mebendazole enhances cisplatin's effect on suppressing cell proliferation and promotes differentiation of head and neck squamous cell carcinoma (HNSCC). Oncotarget 2017;8:12968–12982. [PubMed: 28099902]
29. Pantziarka P, Bouche G, Meheus L, et al. Repurposing Drugs in Oncology (ReDO)—Mebendazole as an anti-cancer agent. Ecancermedicalscience 2014;8:443. [PubMed: 25075217]
30. Larsen AR, Bai RY, Chung JH, et al. Repurposing the antihelmintic mebendazole as a hedgehog inhibitor. Mol CancerTher 2015;14:3–13.
31. Cochrane CR, Szczepny A, Watkins DN, et al. Hedgehog signaling in the maintenance of cancer stem cells. Cancers (Basel) 2015;7:1554–1585. [PubMed: 26270676]
32. Lewis MT, Visbal AP. The hedgehog signaling network, mammary stem cells, and breast cancer: Connections and controversies. Ernst Schering Found Symp Proc 2006;181–217. [PubMed: 17939302]
33. Gottlieb E, Armour SM, Harris MH, et al. Mitochondrial membrane potential regulates matrix configuration and cytochrome C release during apoptosis. Cell Death Differ 2003;10:709–717. [PubMed: 12761579]
34. Pavlopoulou A, Oktay Y, Vougas K, et al. Determinants of resistance to chemotherapy and ionizing radiation in breast cancer stem cells. Cancer Lett 2016;380:485–493. [PubMed: 27450721]
35. Hou ZJ, Luo X, Zhang W, et al. Flubendazole, FDA-approved anthelmintic, targets breast cancer stem-like cells. Oncotarget 2015; 6:6326–6340. [PubMed: 25811972]
36. Ichikawa Y, Ghanefar M, Bayeva M, et al. Cardiotoxicity of doxorubicin is mediated through mitochondrial iron accumulation. J Clinical Invest 2014;124:617–630. [PubMed: 24382354]

37. Octavia Y, Tocchetti CG, Gabrielson KL, et al. Doxorubicin-induced cardiomyopathy: From molecular mechanisms to therapeutic strategies. J Mol Cell Cardiol 2012;52:1213–1225. [PubMed: 22465037]
38. Zhu Q, Kirova YM, Cao L, et al. Cardiotoxicity associated with radiotherapy in breast cancer: A question-based review with current literatures. Can Treatment Rev 2018;68:9–15.
39. Hamilton GR, Rath B. Repurposing of anthelminthics as anticancer drugs. Oncomedicine 2017;2:142–149.
40. Simbulan-Rosenthal CM, Dakshanamurthy S, Gaur A, et al. The repurposed anthelmintic mebendazole in combination with trametinib suppresses refractory NRASQ61K melanoma. Oncotarget 2017; 8:12576–12595. [PubMed: 28157711]
41. Kralova V, Hanusova V, Stankova P, et al. Antiproliferative effect of benzimidazole anthelmintics albendazole, ricobendazole, and flubendazole in intestinal cancer cell lines. Anticancer Drugs 2013;24: 911–919. [PubMed: 23884106]
42. Spagnuolo PA, Hu J, Hurren R, et al. The antihelmintic flubendazole inhibits microtubule function through a mechanism distinct from Vinca alkaloids and displays preclinical activity in leukemia and myeloma. Blood 2010;115:4824–4833. [PubMed: 20348394]
43. Sasaki J, Ramesh R, Chada S, et al. The anthelmintic drug mebendazole induces mitotic arrest and apoptosis by depolymerizing tubulin in non-small cell lung cancer cells. Mol Cancer Ther 2002;1: 1201–1209. [PubMed: 12479701]
44. Laclette JP, Guerra G, Zetina C. Inhibition of tubulin polymerization by mebendazole. Biochem Biophys Res Commun 1980;92:417–423. [PubMed: 7356473]
45. Lacey E, Watson TR. Structure-activity relationships of benzimidazole carbamates as inhibitors of mammalian tubulin, in vitro. Bio-chem Fharmacol 1985;34:1073–1077.
46. Gull K, Dawson PJ, Davis C, et al. Microtubules as target organelles for benzimidazole anthelmintic chemotherapy. Biochem Soc Trans 1987;15:59–60. [PubMed: 3556740]
47. Pinto LC, Soares BM, Pinheiro Jde J, et al. The anthelmintic drug mebendazole inhibits growth, migration and invasion in gastric cancer cell model. Toxicol In Vitro 2015;29:2038–2044. [PubMed: 26315676]
48. De Witt M, Gamble A, Hanson D, et al. Repurposing mebendazole as a replacement for vincristine for the treatment of brain tumors. Mol Med 2017;23:50–56. [PubMed: 28386621]
49. Kubota Y, Iwamoto T, Seki T. The interaction of benzimidazole compounds with DNA: Intercalation and groove binding modes. Nucleic Acids Symposium Ser 1999;53–54.
50. Bhattacharya S, Chaudhuri P. Medical implications of benzimidazole derivatives as drugs designed for targeting DNA and DNA associated processes. Curr Med Chem 2008;15:1762–1777. [PubMed: 18691037]
51. Arjmand F, Parveen S, Afzal M, et al. Synthesis, characterization, biological studies (DNA binding, cleavage, antibacterial and topoisomerase I) and molecular docking of copper(II) benzimidazole complexes. J Photochem Photobiol B 2012;114: 15–26. [PubMed: 22695227]
52. Sasagawa S, Nishimura Y, Kon T, et al. DNA damage response is involved in the developmental toxicity of mebendazole in zebrafish retina. Front Pharmacol 2016;7:57. [PubMed: 27014071]
53. Bai RY, Staedtke V, Rudin CM, et al. Effective treatment of diverse medulloblastoma models with mebendazole and its impact on tumor angiogenesis. Neuro Oncol 2015;17:545–554. [PubMed: 25253417]
54. Bai RY, Staedtke V, Wanjiku T, et al. Brain penetration and efficacy of different mebendazole polymorphs in a mouse brain tumor model. Clin Cancer Res 2015;21:3462–3470. [PubMed: 25862759]

Summary

Triple-negative breast cancer (TNBC) remains one of the most challenging breast cancers to treat, despite aggressive treatment approaches, including radiation therapy. In this study, a common anthelminthic drug, mebendazole, is shown to deplete breast cancer stem cells in a TNBC model and act as a potent radiosensitizer in vitro and in vivo. These results strongly support the repurposing of mebendazole as a radiosensitizer for the treatment of patients with TNBC, in combination with radiation therapy.

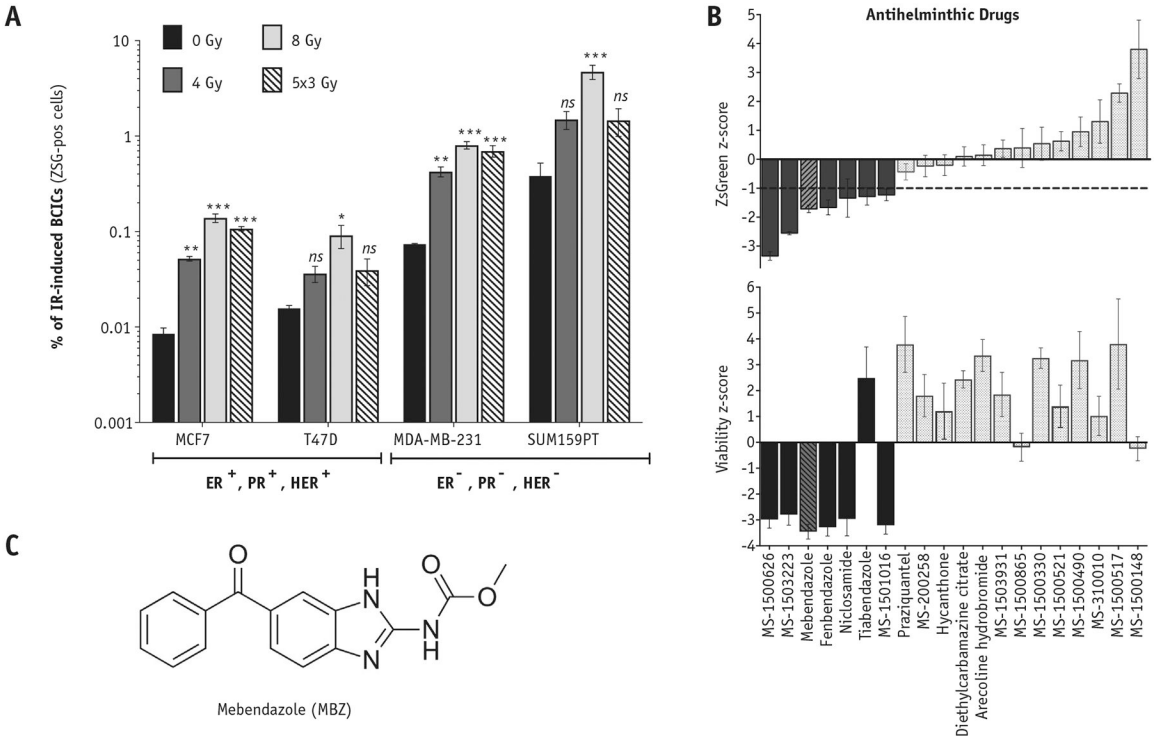

Fig. 1.

Select anthelminthic drugs can inhibit radiation-induced dedifferentiation in triple-negative breast cancer. (A) Breast cancer cells derived from luminal breast cancer (MCF7 and T47D) and triple-negative breast cancer (MDA-MB-231 and SUM159PT) were depleted of BCICs via high-speed FACS. BCICs were identified via a fluorescent reporter system that reports for low proteasome activity (ZsGreen-cODC, ZSG-pos) in BCICs.[8] The sorted, noninitiating cells (ZSG-neg) received different doses of irradiation, and 5 days later the percentage of spontaneous (0 Gy) and radiation-induced (4 Gy, 8 Gy, and 5 daily fractions of 3 Gy) ZSG-pos BCICs was estimated via flow cytometry. Paired, 2-tailed *t* test: **P* < .001; ***P* < .001; ****P* < .0001; *ns*, not significant. (B) Drugs with anthelminthic properties were tested in a low-throughput assay for the ability to inhibit radiation-induced dedifferentiation of noninitiating (ZSG-neg) breast cancer cells into IR-induced BCICs (induced-ZSG-pos) using the SUM159PT TNBC line. SUM159PT-ZSG-neg cells were isolated via high-speed FACS, plated on 384-well plates containing 10 μM of the anthelminthic drugs, and irradiated with 8 Gy the following day. After 5 days, the cells were stained with the viability dye, Hoechst 33342, and the number of dedifferentiated ZSG-pos cells (B, top panel) and viable cells (B, bottom panel) was determined via a laser-scanning cytometer. The <mi> scores were calculated based on the DMSO control values. MBZ (striped bars) efficiently inhibited radiation-induced dedifferentiation while also resulting in significant toxicity to the bulk cell population. (C) The structure of MBZ. *Abbreviations:* BCICs = breast cancer-initiating cells; DMSO = dimethyl sulfoxide; FACS = fluorescence activated cell sorting; IR = ionizing radiation; MBZ = mebendazole.

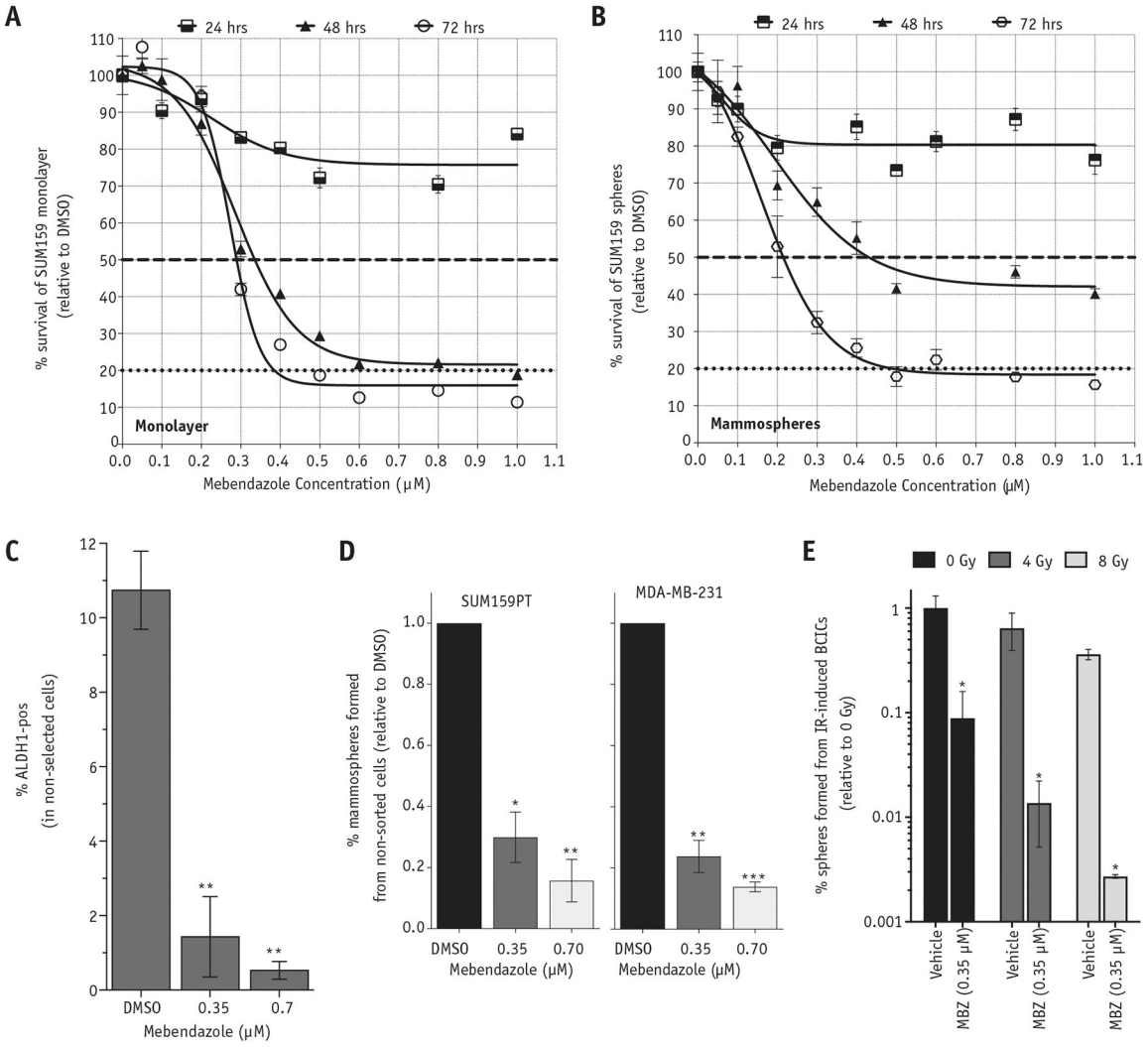

Fig. 2.

MBZ is toxic to differentiated and stem-cell enriched cultures of triple-negative breast cancers and inhibits their self-renewal capacity. SUM159PT cells were plated on 96-well plates as monolayers (A) or mammosphere cultures enriched for BCICs (B) and treated with increasing doses of MBZ. Cell viability was determined at 24, 48, and 72 hours after MBZ treatment via ATPlite 1step Luminescence Assay, and the relative luminescence units are expressed as percentage of DMSO controls. EC50 values for monolayer and mammospheres were estimated (dashed horizontal lines). (C) SUM159PT monolayer cultures were treated with a single dose of MBZ at the indicated concentrations, and 5 days later the percentage of BCICs was determined based on ALDH1 activity (ALDH1-pos) using the ALDEFLUOR assay. Paired, 2-tailed *t* test: $^{**}P < .001$. (D) SUM159PT and MDA-MB-231 cells were plated in serum-free mammosphere media in low-adhesion, 96-well plates, treated with a single dose of MBZ at the indicated concentrations, and allowed to form mammospheres for 2 weeks. The number of mammospheres formed was counted and expressed as a percentage of the number of cells plated. Paired, 2-tailed *t* test: $^{*}P < .01$, $^{**}P < .001$, $^{***}P < .0001$. E, ZSG-pos BCICs from SUM159PT-ZsGreen-cODC line were depleted via high-speed FACS

and plated on 6-well plates, treated with a single dose of MBZ (0.35 μM), and irradiated 1 hour later. After 5 days, cells were removed and plated in a mammosphere-forming assay in serum-free conditions, and the percentage of dedifferentiated cells able to form mammospheres was determined after 2 weeks. Unpaired, 2-tailed *t* test: ***$P < .0001$.

Abbreviations: ALDH1 = aldehyde dehydrogenase 1; BCICs = breast cancer-initiating cells; DMSO = dimethyl sulfoxide; FACS = fluorescence activated cell sorting; IR = ionizing radiation; MBZ = mebendazole.

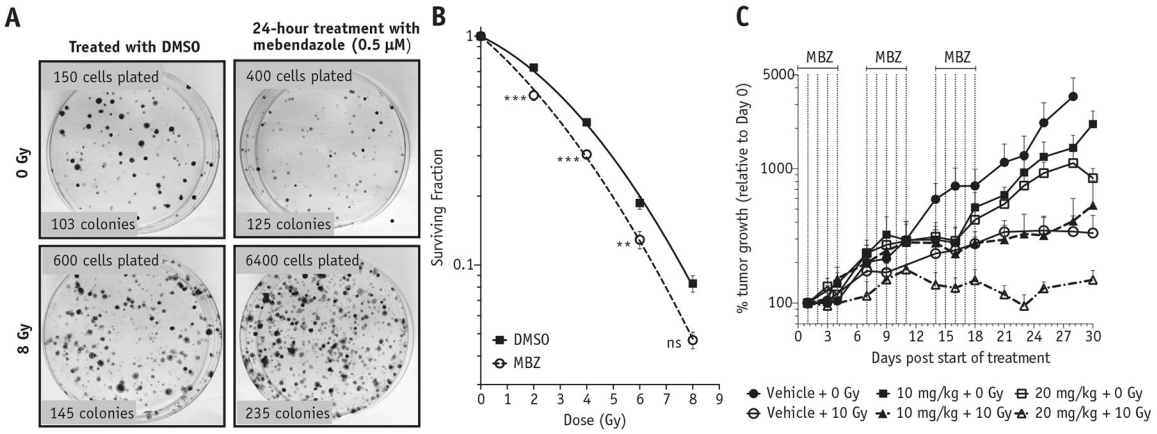

Fig. 3.

MBZ radiosensitizes triple-negative breast cancer in vitro and in vivo. (A) SUM159PT cells were treated with MBZ (0.5 μM) for 24 hours. On the next day, the drug was removed, and cells were detached, irradiated at different doses, and plated in a clonogenic survival assay. Colonies of more than 50 cells were stained with crystal violet and counted 3 weeks later (B). Data points in (B) are means of 4 biological repeats ± 1 SEM. There was a statistically significant change in the alpha and beta parameters obtained from a linear-quadratic fit between the control and treated groups. A 2-way analysis of variance statistical test for each irradiation dose was also performed: $^{**}P < .001$, $^{***}P < .0001$. (C) SUM159PT tumors were implanted subcutaneously on the thighs of NSG mice. When the tumors reached an average diameter of 5 mm, they were irradiated with a single dose of 10 Gy followed by administration of MBZ intraperitoneally for 5 days, with 2 days off, for 3 weeks (n = 4–6). Results are the average of biological replicates, and error bars represent 1 SEM. Dotted lines indicate the MBZ treatment schedule. The tumor volumes were determined every other day and plotted as a percentage of tumor growth (note logarithmic scale for y-axis).

Abbreviations: DMSO = dimethyl sulfoxide; MBZ = mebendazole; SEM = standard error of the mean.

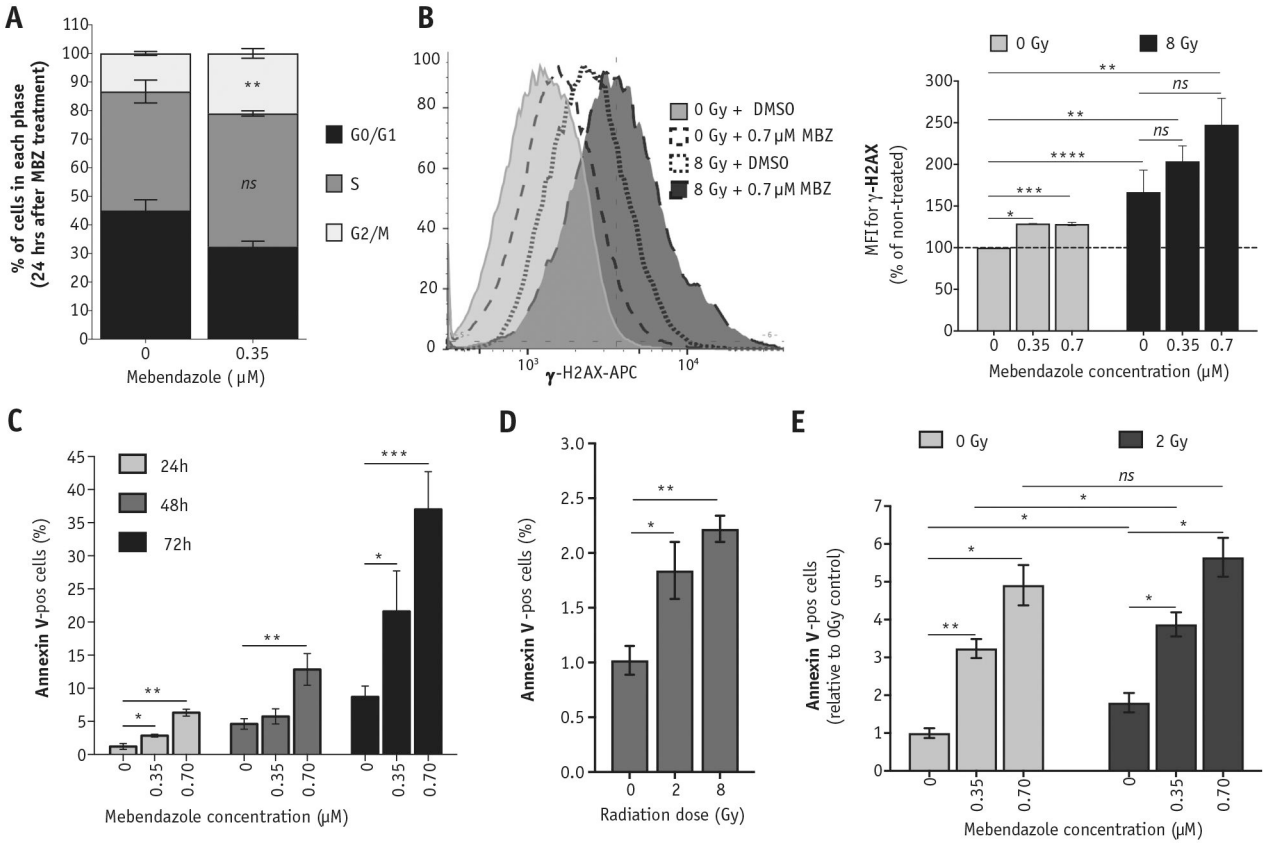

Fig. 4.

Exposure to MBZ induces double-strand breaks, apoptosis, and cell cycle arrest. SUM159PT cells were treated with a single dose of MBZ at the indicated concentrations. (A) Cell cycle distribution was analyzed 24 hours after MBZ treatment using propidium iodide staining. (B) Twenty-four hours after MBZ treatment, cells were exposed to a single dose of IR (8 Gy). Thirty minutes after exposure to IR (or 24 hours after MBZ treatment), cells were removed and stained with anti-γ-H2AX-APC to determine the relative number of double-strand breaks (top). The MFI is plotted for the average of 3 independent experiments (bottom). Unpaired, 2-tailed *t* test: **P* < .01, ***P* < .001, ****P* < .0001, *****P* < .00001, *ns*, not significant. (Bottom panel) Representative FACS histograms. (C-E) The percentage of cells staining positive for Annexin-V was determined via flow cytometry. (C) The percentage of Annexin-V-pos cells was determined at 24, 48, and 72 hours after MBZ treatment. (D) The percentage of Annexin-V-pos cells was determined at 24 hours after the indicated doses of radiation. (E) Cells were treated with the indicated doses of MBZ and, 24 hours later, exposed to 2 Gy. The percentage of Annexin-V-pos cells was determined 24 hours after irradiation. Paired, 2-tailed *t* test: ns, not significant, **P* < .01, ***P* < .001.

Abbreviations: FACS = fluorescence activated cell sorting; IR = ionizing radiation; MBZ = mebendazole; MFI = mean fluorescent intensity.